Design of a nickel-base superalloy using a neural network

B.D. Conduit

Rolls-Royce plc, PO Box 31, Derby, DE24 8BJ, United Kingdom

N.G. Jones

Rolls-Royce UTC, 27 Charles Babbage Road, Cambridge, CB3 0FS, United Kingdom

H.J. Stone

Rolls-Royce UTC, 27 Charles Babbage Road, Cambridge, CB3 0FS, United Kingdom

G.J. Conduit

Cavendish Laboratory, J.J. Thomson Avenue, Cambridge, CB3 0HE, United Kingdom

Abstract

A new computational tool has been developed to model, discover, and optimize new alloys that simultaneously satisfy up to eleven physical criteria. An artificial neural network is trained from pre-existing materials data that enables the prediction of individual material properties both as a function of composition and heat treatment routine, which allows it to optimize the material properties to search for the material with properties most likely to exceed a target criteria. We design a new polycrystalline nickel-base superalloy with the optimal combination of cost, density, γ' phase content and solvus, phase stability, fatigue life, yield stress, ultimate tensile strength, stress rupture, oxidation resistance, and tensile elongation. Experimental data demonstrates that the proposed alloy fulfills the computational predictions, possessing multiple physical properties, particularly oxidation resistance and yield stress, that exceed existing commercially available alloys.

Keywords: Neural network; materials design; nickel-base superalloy

Despite the central importance of materials in enabling new technologies, historically the only way to develop new materials has been through experiment driven trial and improvement [1]. This means that commercially available alloys are the result of many years of empirical development, and whilst they have good properties, they do not necessarily offer the right balance of properties needed for specific engineering applications. The capability to discover materials computationally has the potential to empower engineers to utilize materials optimized for their application [2]. The development of new algorithms

and a surge in computing power has enabled the screening of large numbers of prospective compositions with first principles calculations [1]. Designing alloy compositions to identify which best fulfill the target criteria has previously been attempted with a Pareto set [3–5], a principal component analysis [6], robust design [7], and the orthogonal optimization of different properties [2, 8–11]. In this paper, we develop a new computational tool that combines experimental data with computational thermodynamic predictions [12] to rapidly, reliably, and robustly identify the alloy composition that is most likely to meet a multi-criterion specification [13].

We use the tool to propose a new nickel-base superalloy [14]. A nickel-base superalloy is an ideal case study for real-life materials design, because of the need to obtain the optimal balance of many properties, including physical and thermodynamic requirements, with a special focus on improving the critical properties of yield stress and oxidation resistance. This case study not only serves as an independent test of the alloy design approach, but moreover leads to a potentially commercially viable alloy.

In the first part of this paper, the computational tools developed to predict both the expected value and the associated uncertainty in a material's physical properties are described. The computational tools are used to evaluate the likelihood that a proposed alloy composition will satisfy the design criteria, and to then select the composition most likely to fulfill the design criteria. This means that we are proposing the alloy that is most likely to succeed in experimental verification, and, therefore, be of most use to the engineer. The efficiency of this approach is demonstrated in the second section of the paper where we present experimental results for the properties of the proposed new alloy, proving that is has a combination of properties that surpass commercially available alternatives.

1. Formalism

The goal of the concurrent materials design formalism is to predict a composition and processing variables that are most likely to fulfill the multi-criteria target specification such as a maximum permissible cost and minimum allowed yield stress. First, predictive models are constructed for each property, second, these models are used to calculate the probability that a proposed composition fulfills the target specification, and finally search composition space for the alloy most likely to fulfill the specification.

The properties that were optimized in the design of the nickel-base superalloy are shown in Table (1). With properties depending on contrasting length scales, different calculation methods were adopted that are referenced in the tables. For some properties including cost and density, physically based models were adopted: density was calculated as a weighted average of the densities of the elements comprising the alloy, cost was a weighted average of the prices of the elements comprising the alloy plus a fixed charge for the preparation and heat treatments. Two methods can be used to calculate phase stability, the first using the PhaComp method [15] is evaluated from the average energy levels

Property	Approach	Points	Target
Cost	Physical	[90]	$< 33.7\,\$\,\mathrm{kg}^{-1}$
Density	Physical	[27]	$< 8281\,\mathrm{kg\,m}^{-3}$
γ' content	CALPHAD	[12, 28]	$< 50.4\,\mathrm{vol}\,\%$
Phase stability	CALPHAD	[12]	$> 99.0\,\mathrm{vol}\,\%$
Fatigue life at 500MPa	Neural net	15105[29, 30]	$> 10^{3.9}$ cycles
Yield stress	Neural net	6939[31–83]	$> 752.2\,\mathrm{MPa}$
Ultimate tensile strength	Neural net	6693[31–83]	$> 960.0\,\mathrm{MPa}$
300hr rupture	Neural net	10860[31–83]	$> 674.5\,\mathrm{MPa}$
Cr activity at 800℃	Neural net	915[84]	> 0.14
γ' solvus	CALPHAD	[12]	$> 983\,^{\circ}\mathrm{C}$
Tensile elongation	Neural net	2248[31–83]	$> 11.6\,\%$

Table 1: The approach used to predict properties, number of experimental points used to train the nickel-base superalloy neural network models, references for the data, and the target specification.

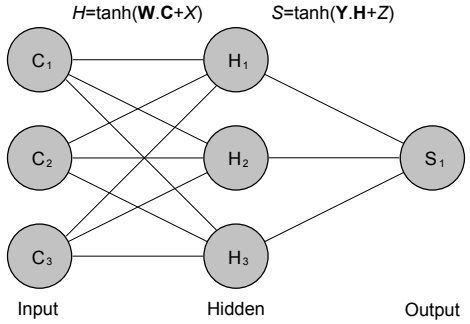

Figure 1: (Color online) Schematic representation of the neural network.

of d-orbitals (M_d) within the transition metals in the alloy, a $M_\mathrm{d} < 0.98$eV indicates that there will be acceptably low formation of topologically closed packed phases. M_d can be evaluated with little computational expense for the composition space search; the final composition was cross-checked with the CALPHAD method [16], with data sourced from the TTNI8 database [12].

Several properties cannot be reliably calculated from computer modeling. Instead, for the fatigue life, yield stress, ultimate tensile strength, rupture, and tensile elongation a database of experimental results as a function of composition and heat treatment was compiled from the sources referenced in Table (1). A neural network model was constructed that predicts the physical properties, $\mathbf{S}(\mathbf{C})$, for composition, $\mathbf{C}$. The form of the neural network is shown in Figure 1. The network takes three input variables $C_{1,2,3}$, the links act on the variables through the indicator function $H_{1,2,3} = \tanh(\mathbf{W_{1,2,3}} \cdot \mathbf{C} + X_{1,2,3})$, to transform them into three hidden node values $H_{1,2,3}$. The hidden nodes are again combined by indicator functions $\tanh(\mathbf{Y} \cdot \mathbf{H} + Z)$ to give the final output value S_1. This network, shown in Figure 1, has free variables $W_{11,12,13,21,22,23,31,32,33}$, $X_{1,2,3}$,

$Y_{1,2,3}$ and Z. In the design of the nickel-base superalloy there are up to $N_{\rm D} = 25$ input values $C_{1,2,\cdots,25}$ covering both composition and heat treatments. The free variables are optimized by minimizing the reduced chi-squared statistic over the preexisting data

$$\chi^2_{\rm red} = \frac{1}{N - (2 + N_{\rm D})N_{\rm H} - 1} \sum_{j=1}^{N} \frac{(S_j - s_j)^2}{\sigma_j^2} \,. \tag{1}$$

where N is the number of data points of values $\{s\}$ and experimental uncertainty $\{\sigma\}$ available for training. The statistic divides by the number of free variables $N - (2 + N_{\rm D})N_{\rm H} - 1$ that includes the number of hidden nodes $N_{\rm H}$. We found that typically $N_{\rm H} = 3$ hidden nodes gave the minimal reduced chi-squared statistic. A separate system of neural networks with its own optimizable parameters was constructed for each output $\mathbf{S}_i$. To evaluate the uncertainty in the predictions, a committee of $M = 64$ neural network models, labeled $j \in \{1 \dots M\}$, was constructed using the Bayesian bootstrap approach [17, 18] that delivers predictions $\mathbf{S}(\mathbf{C})_j$. Each neural network model was constructed by associating random weights with the input data, which deliver a range of outputs correctly distributed to reflect the underlying uncertainty in the networks due to the limited input data [17, 18]. For the proposed composition, the average value over the models gives the predicted physical value $\mathbf{V_C} = \frac{1}{M} \sum_{j=1}^{M} \mathbf{S}_{\mathbf{C},j}$, and the uncertainty was found through the covariance matrix $\mathbf{\Sigma_C} = \sum_{j=1}^{M} (\mathbf{S}_{\mathbf{C},j} - \mathbf{V_C})(\mathbf{S}_{\mathbf{C},j} - \mathbf{V_C})^{\rm T}$ [19]. The knowledge of uncertainty is crucial as it allows the designer to balance the risk of materials with lower uncertainty but are less capable versus promising but speculative alloys.

With a prescription to calculate the separate properties of a material, a single merit index is defined to describe how well the material satisfies the design criteria that can then be optimized. The neural network models offer a unique insight into the inevitable uncertainty that exists in the predictions based on experimental data. The uncertainty means that the probability that a putative composition will satisfy the target design criterion, $\mathbf{T}$, is $P_{\mathbf{C}} = \Phi[\mathbf{\Sigma}_{\mathbf{C}}^{-1}(\mathbf{V_C} - \mathbf{T})]$, where we assume that uncertainties are normally distributed so Φ is the multivariate cumulative normal distribution function [19]. Combining the individual property probabilities can dramatically reduce the probability that the overall alloy will fulfill the whole specification: for example, if the material has a 50% probability of fulfilling each of the ten specified design criteria, the overall probability that is fulfills all criteria is $0.5^{10} \approx 0.001$, so 0.1%. Therefore, it is crucial that the probability of the material meeting the conformance specification is maximized. To achieve this, the logarithm of the probability $\log(P_{\mathbf{C}})$ is maximized to ensure that, in the region where the material is predicted to not satisfy the specification, the optimizer runs up a constant gradient slope that persistently favors the least optimized property.

The design tool's use of uncertainty and probability is vital here: the further the composition is from existing experimental data or the greater the uncertainty in the experimental data, the larger the uncertainty. The tool can therefore be

allowed to explore the entire range of compositions, and as soon as it is extrapolating far beyond any available experimental data points the uncertainty will grow, naturally bounding the range of compositions from which new alloys may be reliably predicted. The use of likelihood also allows the tool to explore and select the ideal compromise between material properties, which is inaccessible to methods that do not account for likelihood such as a principal component analysis [6] and robust design [7]. Similarly, the design tool may interpolate between experimental data, exploring more compositions than would be accessible by an experimentally driven search. Using a neural network to interpolate allows us to capture deeper correlations than linear regression methods such as a principal component analysis [6].

As well as predicting material properties, the tool must optimize them. Previous optimization techniques included running over a pre-determined grid of compositions, and then sieving them with orthogonal [2, 8–11], or a Pareto set [3–5]. However the expense of these methods scales exponentially with the number of design variables rendering them impractical. Another approach is the use of genetic algorithms [20, 21]. However, this approach is not mathematically guaranteed to find the optimal solution [22, 23], and it displays poor performance in high dimensional problems [22, 23]. Both of these disadvantages can be overcome by adopting a simulated annealing based approach. With this approach, a step length can be used that is comparable to the accuracy with which a material could be manufactured, this is approximately 0.1 wt. % for each element within the entire composition excluding the possibility of microsegregation. The temperature is selected so that a fraction of 0.267 steps are accepted, the optimum to explore a multidimensional space [24]. If too few steps are being accepted the tool reduces the temperature parameter, if too many then temperature increases. This allows the tool to rapidly explore the design variable space whilst not getting stuck in local minima. Using this approach, searches of over $\sim 10^8$ sets of design variables are accomplished in ~ 1 hour to identify an optimal material.

2. Results and discussion

Nickel-base superalloys display remarkable high temperature mechanical properties and environmental resistance. They are used in the gas turbine engines of the aerospace, marine, and power generation industries, meaning that there is significant commercial and environmental motivation to develop improved alloys to enable more efficient engines to be designed and emissions reduced [25]. The demanding operating conditions at the heart of an engine mean that a superalloy must simultaneously satisfy at least the eleven target properties shown in Table (1). As nickel-base superalloys have been intensely studied since the 1930's [12, 26–84] and there are over 120 commercially available alloys for different specialist applications, the optimizing program showed that there is no single composition that offers properties that exceeds all of the alloys available. Instead the materials design formalism offers the capability of finding the ideal compromise between different properties. To demonstrate this capability, an

Optimal composition (wt. %)			
Mn	0.2±0.2	Cr	15.8±0.7
Co	20.0±0.9	Ti	3.0±0.2
Mo	0.5±0.3	Fe	3.9±0.4
W	0.5±0.3	Si	0.2±0.2
Ta	4.9±0.3	Zr	0.18±0.03
Nb	1.1±0.2	B	0.06±0.01
Al	2.4±0.2	C	0.02±0.01
Ni	Balance		
T	900℃	t	30 hr

Table 2: The proposed nickel-base superalloy composition (wt. %) and heat treatment routine with the design tolerance of all design variables that are predicted to fulfill the target specification.

alloy has been sought that improves the real-life limiting factors [85] of yield stress at 800℃ and oxidation resistance, without greatly sacrificing any other property. The majority of properties are set by the engineering requirements of the application and to exceed the properties of RR1000 and Udimet720. For example, elongation is set at the lower bound of the elongation of Udimet720 of 11.6%, as the alloy only needs a sufficient ductility for damage tolerance in a turbine disc alloy, so this target is set to allow additional freedom to achieve other property targets. The γ' phase content target is set to control the solvus temperature below 1150℃, alloys which exceed this temperature such as Alloy 10 are known to be difficult to process and suffer from quench cracking [86]. The alloy has then been benchmarked against the contemporary alloys Udimet720 (Rolls-Royce AE3007™ engine), LSHR (NASA proposed disc alloy), Rene104 (General Electric GEnx engine), and RR1000 (Rolls-Royce Trent 1000 engine).

Models for the properties shown in Table (1) were constructed, using data from the references highlighted. The yield stress model focused on arc melted alloys that are readily experimentally accessible – in commercial disc applications the alloy would be powder processed, which typically leads to a $\sim 20\%$ higher yield stress through better grain size and homogeneity control [71]. Phase stability was defined by the volume fraction of the desirable γ and γ' phases present after exposure at 750℃ for 1000 hours, this is equivalent to compositions with a value of $M_{\mathrm{d}} < 0.98$eV that are likely to remain mostly free of undesirable phases at exposures of 750℃ for 1000 hours. Fatigue performance was taken to be the number of cycles the sample could withstand of a 500 MPa peak stress oscillating at 60 Hz. Rupture was the maximum stress that the alloy can withstand at 700℃ for 300 hours. Cr activity was $\exp[(\mu - \mu_{\mathrm{Cr}})/RT]$ where μ_{Cr} is the chemical potential of Cr in the alloy and which ultimately forms a Cr_2O_3 layer that protects against further oxidation and corrosion [84].

The target properties for the Ni superalloy are shown in Table (1). We focus on searching for an alloy that has a better high-temperature yield strength, to allow it to be used in the next generation of engines with higher operating temperature and also better oxidation resistance than previous alloys to increase

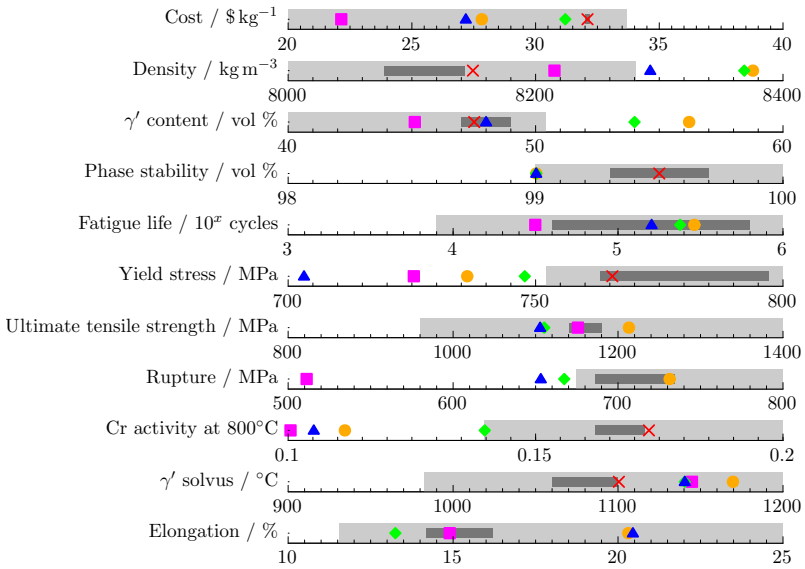

Figure 2: Summary of properties for the Ni superalloy. For each listed property the gray box refers to the acceptable target properties, the dark gray is the three-sigma uncertainty on the theoretical prediction. The points refer to experimentally measured values with × V210A where measured, ■ refers to Udimet720, ● LSHR, ♦ Rene104, and ▲ RR1000.

engine service intervals. Therefore, an alloy is sought that has a target yield strength that exceeds 752 MPa, greater than the best in the sample set, Rene104. The alloy must also have higher levels of chromium activity than previous alloys to promote improved oxidation resistance. The targets were set so that the alloy should then be competitive on all other properties. These models allowed a composition to be proposed along with an appropriate heat treatment schedule that has a 20% probability of fulfilling the target specification. The theoretical predictions, shown in Figure 2, all fall within the required target specification. This new alloy is denoted V210A, the composition of which is given in Table (2).

2.0.1. Analysis of proposed alloy

The aim of the alloy design tool is to select the alloy with the highest probability of exceeding all the targets. Examining the probability of an alloy satisfying the design targets exposes the compromise that has been made between the physical properties stress rupture, phase stability, thermal expansivity, yield stress, and ultimate tensile strength.

An example of the compromises that must be made between properties is presented in Figure 3(a) in which the probability of three compositionally similar alloys (Alloy A, Alloy B, and Alloy V210A) exceeding various property targets are shown as a function of yield stress. All three alloys are predicted to have a high yield stress, in excess of the target specification. However, the probability that they meet the other target properties varies considerably. Alloy

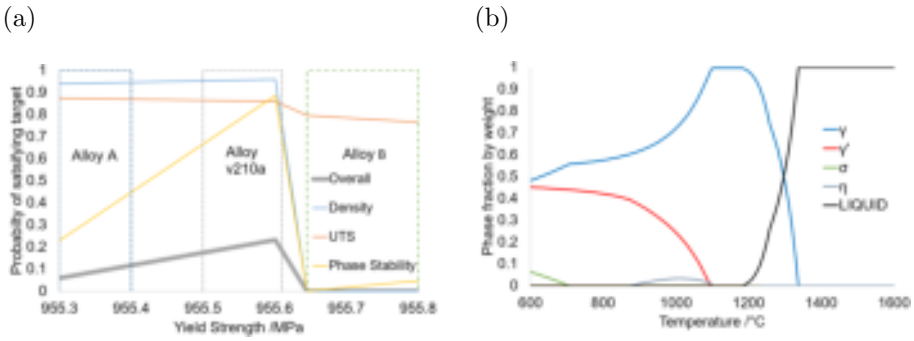

Figure 3: (Color online) (a) The variation of the probability of satisfying the overall (gray), density (blue), ultimate tensile strength (red), and phase stability target (yellow) as a function of yield strength of the alloy. As well as V210A, two additional alloys, A and B, are described in the text. (b) The phase fraction of the γ (blue), γ' (red), σ (green), η (gray), and liquid (black) phases for the alloy V210A.

A is predicted to have a high probability of exceeding the density and ultimate tensile strength targets but falls short in respect to phase stability. Alloy B has a high probability of exceeding the UTS target but a poor prediction in terms of phase stability and density. Alloy V210A has a high probability of exceeding all three property targets plotted. Thus, when the properties are combined to give an overall likelihood of meeting all the targets, V210A has a probability which exceeds both that of Alloy A and Alloy B. It should be noted that, because the plot shows how the probability varies with a single property, yield stress, rather than composition, there is a sharp peak in property space.

Physical properties of Ni alloys are controlled not only by composition but also with the operating temperature. Therefore, to understand the variation of physical properties, in Figure 3(b) we examine the predicted mass fraction of phases as a function of temperature for the alloy V210A. The γ' solvus temperature is predicted to be 1100℃. Between the temperatures of 870-1100℃, a small percentage of η phase (Ni_3Ti) is predicted to form; if the alloy is processed above the solvus temperature and operated at < 850℃ then the volume fraction observed in the alloy should be close to zero. Out of all the deleterious phases that can be formed within V210A, the σ phase is predicted to form at the highest temperature, yet it is < 700℃; below these temperatures the kinetics of diffusion within the alloy will be slow enough to prevent formation of this phase. The σ phase forms a "basket weave" morphology, which has a severe impact on mechanical properties that affects many commercially available alloys. The rapidly varying phase stability of the alloy, as indicated in Figure 3(a), means that the alloy properties are expected to vary rapidly across property space.

Having seen how the yield stress, phase stability, ultimate tensile strength, and density can act in counter directions it is appropriate to examine how the probabilities of all the properties vary in tandem. Therefore, pairs of properties

have been selected and examined to elucidate the compromise that must be made between them. For each pair, two graphs are presented, the first graph shows a relief plot of the probability of exceeding the two targets; the second shows the probability of exceeding all the other targets that are taken into consideration.

Stress rupture and phase stability: Figure 4(a) shows the predicted probability of simultaneously satisfying the minimum targets for stress rupture and phase stability. A minimum target for a stress rupture resistance of 500 MPa at 750℃ for 100 hours and a maximum phase stability, $M_{\mathrm{d}} = 0.98\,\mathrm{eV}$ was set. This was set by comparison of the M_{d} values and σ phase formation with existing superalloys.

The regions of high probabilities (bright colors) signify good predicted properties coupled with a low uncertainty due to the higher density of historical data-points around these regions. The lowest probabilities are in the regions where neither target is predicted to be satisfied or where there is a low data density leading to high uncertainty. The rapidly varying pockets of high and low probability are driven by the different properties coming in and out of favor and the phases present vary rapidly across the composition space, as we saw in Figure 3. Since the targets were defined using a normal distribution, at the point 500 MPa, and 0.98 eV the probability of simultaneously satisfy both targets is 0.25. In general, the highest probabilities are around a stress of 850 MPa, and phase stability of 0.95 eV. Creating an alloy with a higher stress rupture resistance and lower phase stability than this becomes increasingly unlikely.

In general, an increase in stress rupture resistance requires additional alloying elements, which results in a decrease in the phase stability [15]. Our probability based approach enables the best compromise between these two competing factors to be found. In addition, it helps establish which elements offer the most effective way of increasing the probability of exceeding the stress rupture target whilst resulting in only a modest decrease in phase stability.

The proposed alloy, V210A, is contained within the large region of high probability well above the minimum stress target, whilst RR1000 and U720Li are just above the target. Rene95 and LSHR have superior stress rupture resistance, but neither Rene95 nor LSHR meet the phase stability target. This graph only shows the probabilities for two properties, most of the high probability region above V210A become infeasible when the other properties are taken into account.

Figure 4(b) shows how the probability distribution with respect to stress rupture and phase stability change when all the other property targets are taken into account. This drastically changes the distribution of probabilities shown in Figure 4(a). Now there are sparse regions of higher probability of exceeding all targets from that obtained when only two properties are considered. V210A is contained within a region of high probability, which we confirm is not noise; firstly, because all of the relief plots, Figure 4, Figure 5, and Figure 6 all show V210A in a region of high probability, secondly because the consideration of probability means that noise has large uncertainty and so would lower the probability, and thirdly by our later experimental verification. The figure correctly

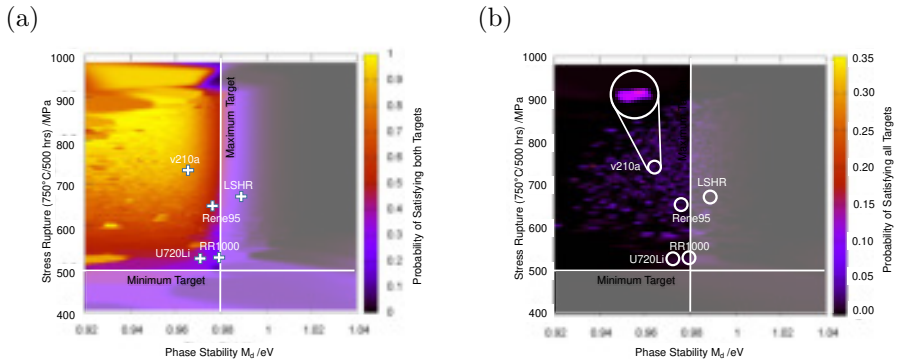

Figure 4: (Color online) (a) The probability of simultaneously satisfying two targets, a maximum phase stability target of 0.98 eV and a minimum stress rupture target of 500 MPa at 750℃ for 100 hours. (b) A relief plot of simultaneously satisfying all of the targets for the material, plotted with respect to phase stability and minimum stress rupture targets.

shows that the alloys LSHR, Rene95, RR1000, U720Li do not fulfill the targets specified. Having seen the impact of the inclusion of the other properties, we next look at the variation of design probability with thermal expansivity and yield stress.

Thermal expansivity and yield stress: Figure 5(a) shows a relief probability plot of thermal expansivity coefficient as a function of yield stress for developing the alloy V210A. Minimum targets of a yield stress of 800 MPa at 750℃ and a maximum thermal expansion coefficient of 17×10^{-6}/K at 750℃ were set. The region with the highest probability of exceeding these two targets is in general at the lowest thermal expansion coefficient and highest yield stress. The thermal expansion coefficient can be improved by adding refractory elements such as Mo, Nb, W and Ta, which will simultaneously improve the yield stress. However, adding these elements will increase the density and reduce phase stability, which makes the majority of the family of alloys infeasible, as shown in the previous graphs.

Figure 5(b) shows how the probability distribution with respect to thermal expansion and yield stress changes when all the other property targets are taken into account. There is not a significant increase on the probability of success with decreasing thermal expansion. Therefore, it may be better to choose an alloy with a relatively high thermal expansion coefficient, as is the case for V210A – which has the highest probability of exceeding all the targets out of the alloys shown. The other alloys shown have similar yield stresses and lower thermal expansion coefficient, but as highlighted previously do not have all the other necessary requirements for the application in question.

Yield stress and ultimate tensile strength: Figure 6(a) shows a relief plot of simultaneously satisfying two targets, a minimum yield stress target of 800 MPa at 750℃ and a minimum ultimate stress target of 950 MPa at 750℃. Figure 6(b) shows how the probability changes if all targets are considered. Now there

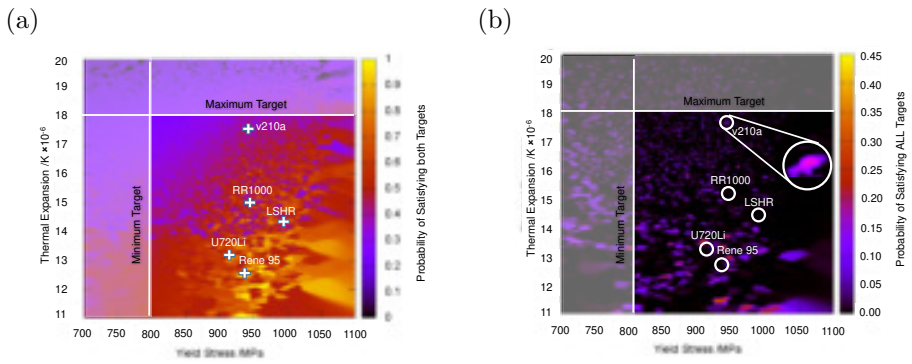

Figure 5: (Color online) (a) A relief plot of simultaneously satisfying two targets, a maximum thermal expansion target of 17×10^{-6}/K at 750℃ and a minimum yield stress of 800 MPa at 750℃. (b) A relief plot of simultaneously satisfying all targets for the material, plotted with respect to thermal expansion and yield stress targets.

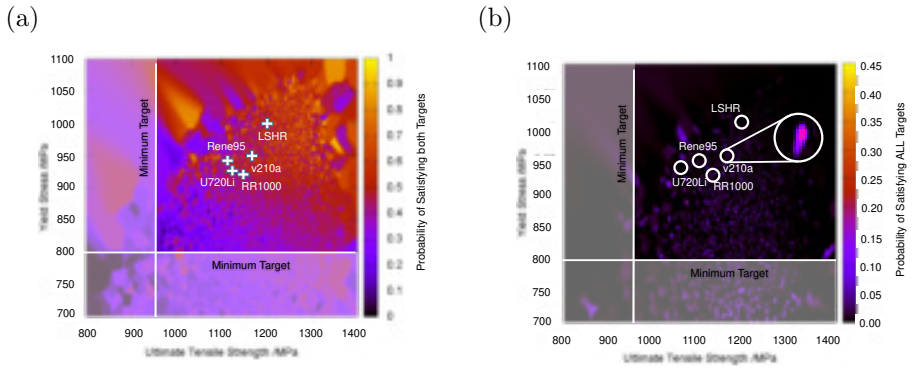

Figure 6: (Color online) (a) A relief plot of simultaneously satisfying two targets, a minimum yield stress target of 850 MPa at 750℃ and a minimum ultimate stress target of 950 MPa at 750℃. (b) A relief plot of simultaneously satisfying all targets for the material, plotted with respect to yield stress and ultimate tensile stress targets.

are many small regions with higher probability of success surrounded by larger regions with a low probability of success. The distribution of probability regions is similar to that seen in the yield stress vs. thermal expansion coefficient.

As can been observed from all of these plots, V210A, sits in a region of high probability which the other alloys do not, and thus is the alloy most likely to meet the targets specified. Obviously, a different set of targets would result in a different distribution of high probability alloys. This highlights the potential advantages of matching the alloy for the specific application.

2.0.2. Experimental verification

Experimental testing was performed to verify the beneficial properties of the proposed alloy, V210A. Starting from pelletized elements with purity greater than 99.9%, the mixture was arc-melted under argon to produce a 50 g ingot through five successive inversion and re-melt cycles. The alloy was then homogenized for 72 hours at 1200℃, followed by the heat treatment in Table (2) of holding at 900℃ for 30 hours. The alloy's yield stress was determined through compression testing on 4 mm diameter, 6 mm long cylindrical samples. Following a 15 minute dwell at the testing temperature a strain rate of $0.001\,s^{-1}$ was applied to measure the 0.2% proof strength. To study the oxidation resistance, a $20 \times 10 \times 0.5$ mm sample, whose surface was ground with 3 µm grit paper was subjected to thermo-gravimetric analysis at 800℃ in air.

The predictions of the phase behavior were verified through secondary electron microscopy, as shown in Figure 7(a). The measured volume fraction of γ' precipitates was determined to be 51%, confirming our predictions, and less than 1% of other deleterious phases were identified. The γ' solvus temperature was determined using metallographic techniques. A small series of ingots were prepared and annealed at ±10℃ of the predicted solvus temperature. The samples were quenched and examined under electron microscopy. Examination of the morphologies of γ' present confirmed that the solvus temperature lay within 10℃ of the predicted result, 1100℃. The experimentally measured density, determined by the Archimedes method, also matched the theoretical prediction. Figure 7(b) shows that the theoretical and experimental yield stress for an arc melted alloy agree within expected uncertainty, and exceed experimentally measured values of the commercial alloy RR1000. The proposed alloy performs well at high temperature due to the retention of γ' precipitate strengthening, as well as solid solution strengthening. For a powder processed alloy, reduced grain size means that the yield stress would be even greater. Figure 7(c) shows that the oxidation resistance agrees with the theoretical prediction and is superior to that of RR1000.

Having examined the experimental results we can summarize and compare all of the seven properties measured (cost, density, γ' content, phase stability, yield stress, Cr activity, and γ' solvus) to the model predictions and the values reported for other commercially available alloys in Figure 2. The properties of V210A are consistent with theoretical predictions, within uncertainty. In particular, V210A exceeds the required targets of yield stress and oxidation resistance, that none of the exemplar commercial alloys Udimet720, LSHR, Rene104, and

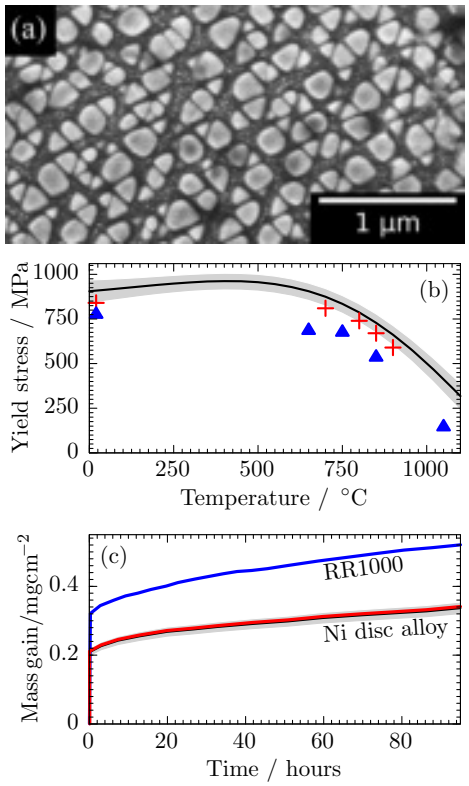

Figure 7: (Color online) (a) Secondary electron micrograph image. (b) V210A yield stress as a function of temperature with black the theoretical prediction for the proposed alloy, along with the uncertainty in gray. The points + show experimental results for the optimal alloy and ▲ RR1000. (c) Oxidation resistance of V210A and RR1000 with temperature. The theoretical predictions are shown in black with uncertainty in gray.

RR1000 simultaneously fulfill. Moreover, the new alloy design tool allows us to see how previous alloys do not have the appropriate compromise between properties, for example Udimet720 is a low cost, lightweight alloy with low γ' content, but it has comparatively poorer stress rupture, yield stress, and oxidation resistance. On the other hand, LSHR fulfills the stress rupture target, but the density and γ' content are arguably too high, along with insufficient oxidation resistance. The ability of the neural network tool to optimize all material properties simultaneously means that the proposed nickel-base superalloy is an ideal candidate for its target application.

3. Conclusions

A new computational alloy design tool was developed that incorporates uncertainty to allow alloys to be designed with the greatest probability of meeting a design specification containing many different material properties. The design tool was used to propose a new nickel-base superalloy alloy most likely to simultaneously fulfill eleven different physical criteria. The tool predicted that the new nickel-base polycrystalline alloy offered an ideal compromise between its properties for disc applications and seven of these properties were experimentally verified, demonstrating that it has better yield stress and oxidation resistance than commercially available alternatives. The tool has also been used to design a nickel-base alloy for a combustor liner [87], and two Mo-based alloys for forging tools [88, 89]. The capability to rapidly discover materials computationally using this approach should empower engineers to rapidly optimize bespoke materials for a given application, bringing materials into the heart of the design process.

Acknowledgments

The authors thank Mark Hardy for useful discussions and acknowledge the financial support of Rolls-Royce plc, EPSRC under EP/H022309/1 and EP/H500375/1, and Gonville & Caius College. There is Open Access to this paper and data available at `https://www.openaccess.cam.ac.uk`.

[1] S. Curtarolo, G.L.W. Hart, M.B. Nardelli, N. Mingo, S. Sanvito, and O. Levy. The high-throughput highway to computational materials design. *Nature Materials*, 12:191, 2013.

[2] C. Kuehmann and G.B. Olson. Computational materials design and engineering. *Materials Science and Engineering*, 25:472, 2009.

[3] T. Bligaard, G.H. Jóhannesson, A.V. Ruban, H.L. Skriver, K.W. Jacobsen, and J.K. Nørskov. Pareto-optimal alloys. *Appl. Phys. Lett.*, 83:4527, 2003.

[4] J. Greeley, T.F. Jaramillo, J. Bonde, I. Chorkendorff, and J.K. Nørskov. Computational high-throughput screening of electrocatalytic materials for hydrogen evolution. *Nature Materials*, 5:909, 2006.

[5] K. Lejaeghere, S. Cottenier, and V. Van Speybroeck. Ranking the stars: A refined pareto approach to computational materials design. *Phys. Rev. Lett.*, 111:075501, 2013.

[6] I. Toda-Caraballo, E.I. Galindo-Nava, and P.E.J. Rivera-Díaz-del Castillo. Unravelling the materials genome: symmetry relationships in alloy properties. *Journal of Alloys and Compounds*, 566:217, 2013.

[7] D.G. Backman, D.Y. Wei, D.D. Whitis, M.B. Buczek, P.M. Finnigan, and D. Gao. Icme at ge: Accelerating the insertion of new materials and processes. *Journal of Materials*, page 3641, 2006.

[8] M. Joo, J. Ryu, and H.K.D.H Bhadeshia. Domains of steels with identical properties. *Mater. Manuf. Process.*, 24:5358, 2009.

[9] W. Xu, P.E.J. Rivera Diaz del Castillo, and S. van der Zwaag. A combined optimization of alloy composition and aging temperature in designing new uhs precipitaition hardenable stainless steels. *Computational Materials Science*, 45:467, 2009.

[10] R.C. Reed, T. Tao, and N. Warnken. Alloys-by-design: application to nickel-based single crystal superalloys. *Acta Materialia*, 57:5898, 2009.

[11] F. Tancret. Computational thermodynamics, gaussian processes and genetic algorithms: combined tools to design new alloys. *Modelling Simul. Mater. Sci. Eng.*, 21:045013, 2013.

[12] J.O. Andersson, T. Helander, L. Höglund, P.F. Shi, and B. Sundman. Thermo-Calc and DICTRA, Computational tools for materials science. *Calphad*, 26:273–312, 2002.

[13] B.D. Conduit and G.J. Conduit. Method and system for designing a material. Patent EP14153898, US 2014/177578, 2014.

[14] B.D. Conduit, G.J. Conduit, H.J. Stone, and M.C. Hardy. A nickel alloy. Patent EP14157622, amendment to US 2013/0052077 A2, 2014.

[15] M. Morinaga, N. Yukawa, H. Adachi, and H. Ezaki. New phacomp and its application to alloy design. In *Superalloys 1984*, pages 523–532. The Minerals, Metals & Materials Society, 1984. ISBN 9780895204783.

[16] L. Kaufman and H. Bernstein. *Computer Calculation of Phase Diagrams*. Academic Press, 1970.

[17] T. Heskes. Practical confidence and prediction intervals. In *Advances in Neural Information Processing Systems 9*, pages 176–182. MIT press, 1997. ISBN 9780262100656.

[18] G. Papadopoulos, P.J. Edwards, and A.F. Murray. Confidence estimation methods for neural networks: a practical comparison. *IEEE Transactions on Neural Networks*, 12:1278, 2001.

[19] L. Wasserman. *All of Statistics: A Concise Course in Statistical Inference*. Springer, 2004. ISBN 978-0387402727.

[20] G.H. Jóhannesson, T. Bligaard, A.V. Ruban, H.L Skriver, K.W. Jacobsen, and J.K. Nørskov. Combined electronic structure and evolutionary search approach to materials design. *Phys. Rev. Lett.*, 88:255506, 2002.

[21] D.P. Stucke and V.H. Crespi. Predictions of new crystalline states for assemblies of nanoparticles: Perovskite analogues and 3-d arrays of self-assembled nanowires. *Nano Letters*, 3:1183, 2003.

[22] L. Ingber and B. Rosen. Genetic algorithms and very fast simulated reannealing: A comparison. *Mathl. Compat. Modelling*, 16:87, 1992.

[23] S.W. Mahfoud and D.E. Goldberg. Parallel recombinative simulated annealing: Agenetic algorithm. *Parallel Computing*, 21:1, 1995.

[24] A. Gelman, G.O. Roberts, and W.R. Gilks. Efficient metropolis jumping rules. *Bayesian Statistics*, 5:599, 1996.

[25] B. Halse. Strategic Research Agenda. Technical report, Advisory Council for Aeronautics Research in Europe, 2004.

[26] C.T. Sims. A history of superalloy metallurgy for superalloy metallurgists. In *Superalloys 1984*, pages 399–419, 1984. ISBN 9780895204783.

[27] R. C. Reed, T. Tao, and N. Warnken. Alloys by Design: Application to Nickel-Based Single Crystal Superalloys. *Acta Materialia*, 57:5898–5913, 2009.

[28] L.D. Connor. *The development of a dual microstructure heat treated Ni-Base superalloy for turbine disc applications*. PhD thesis, University of Cambridge, 2009.

[29] Special Metals. Special metals, 2013. URL `www.specialmetals.com`.

[30] Haynes International, Inc. Haynes international, inc, 2013. URL `www.haynesintl.com`.

[31] C.M. Tomasello, F.S. Pettit, N. Birks, J.L. Maloney, and J.F. Radavich. Precipitation behaviour in aerex 350. In *Superalloys 1996*, pages 145–151. The Minerals, Metals & Materials Society, 1996. ISBN 9780873393522.

[32] J. Radavich and D. Furrer. Assessment of russian p/m superalloy ep741np. In *Superalloys 2004*, pages 381–390. The Minerals, Metals & Materials Society, 2004. ISBN 9780873395762.

[33] C.T. Sims, N.S. Stoloff, and W.C. Hagel. *Superalloys II, High Temperature Materials for Aerospace and Industrial Power*. John Wiley & Sons, Inc, 1987. ISBN 9780471011477.

[34] B. Ewing, F. Rizzo, and C. zurLippe. Powder metallurgy products for advanced gas turbine applications. *Superalloys 1972*, pages 1–12, 1972.

[35] K. Sato and T. Ohno. Development of low thermal expansion superalloy. *Journal of Materials Engineering and Performance*, 2:511–516, 1993.

[36] S. Mannan, S. Patel, and de Barbadillo J. Long term thermal stability of inconel alloys 718, 706, 909, and waspaloy at 593C and 704C. In *Superalloys 2000*, pages 449–458. The Minerals, Metals & Materials Society, 2000. ISBN 9780873394772.

[37] R.J. Mitchell. *Development of a new powder processed Ni-base superalloy for rotor disc application*. PhD thesis, University of Cambridge, 2004.

[38] Z. Meng, G.-C. Sun, M.-L. Li, and X. Xie. The strengthening effect of tantalum in nickel-base superalloys. *Superalloys 1984*, pages 563–572, 1984.

[39] J. Tien, J.P. Collier, and G. Vignoul. The role of niobium and other refractory elements in superalloys. *Superalloy 718*, pages 553–566, 1989.

[40] E.S. Huron, K.P. Bain, D. Mourer, J. Schirra, P.L. Reynolds, and E.E. Montero. The influence of grain boundary elements on properties and microstructures of p/m nickel base superalloys. In *Superalloys 2004*, pages 73–81. The Minerals, Metals & Materials Society, 2004. ISBN 9780873395762.

[41] K.K. Sharma and S.N. Tewari. A high performance wrought nickel-base superalloy El-929. *Journal of Materials Science*, 18:2915–2922, 1983.

[42] C.J. Cowen and P.D Jablonski. Elevated temperature mechanical behavior of new low cte superalloys. In *Superalloys 2008*, pages 201–208. The Minerals, Metals & Materials Society, 2008. ISBN 9780873397285.

[43] L.M. Pike. Development of a fabricable gamma prime (γ') strengthened superalloy. In *Superalloys 2008*, pages 191–199. The Minerals, Metals & Materials Society, 2008. ISBN 9780873397285.

[44] S. Mannan, G.D. Smith, and S. Patel. Thermal stability of inconel alloy 783 at 593C and 704C. In *Superalloys 2004*, pages 627–635. The Minerals, Metals & Materials Society, 2004. ISBN 9780873395762.

[45] D.J. Tillack and H.L. Eiselstein. The invention and definition of alloy 625. In *Superalloys 718, 625 and Various Derivatives*, pages 1–14. The Minerals, Metals & Materials Society, 1991. ISBN 9780873393522.

[46] F. J. Rizzo and J. Radavich. Microstructural characterisation of pm 625-type materials. In *Superalloys 718, 625 and Various Derivatives*, pages 297–308. The Minerals, Metals & Materials Society, 1991. ISBN 9780873393522.

[47] J.H. Moll, G. N. Maniar, and D.R. Muzyka. Heat treatment of 706 alloy for optimum 1200 F stress rupture properties. *Metallurgical and Materials Transactions B*, 2:2153–2160, 1971.

[48] J.R. Brinegar, J.R. Mihalisin, and J. VanderSluis. The effects of tantalum for columbium substitutions in alloy 713c. *Superalloys 1984*, pages 53–61, 1984.

[49] G.K. Bouse and M.R. Behrendt. Mechanical properties of microcast-X alloy 718 fine grain investment castings. *Superalloy 718*, pages 319–328, 1989.

[50] A.R. Braun and J. Radavich. A microstructural and mechanical properties comparison of P/M 718 and P/M TA 718. *Superalloy 718*, pages 623–629, 1989.

[51] K.M. Chang and A.H. Nahm. Rene 220: 100 F improvement over alloy 718. *Superalloy 718*, pages 631–646, 1989.

[52] L. Jackman, G. Smith, A.W. Dix, and M.L. Lasonde. Rotary forge processing of direct aged inconel 718 for aircraft engine shafts. In *Superalloys 718, 625 and Various Derivatives*, pages 125–132. The Minerals, Metals & Materials Society, 1991. ISBN 9780873393522.

[53] J. Schirra, R.H. Caless, and R.W. Hatala. The effect of laves phase on the mechanical properties of wrought and cast + hip inconel 718. In *Superalloys 718, 625 and Various Derivatives*, pages 375–388. The Minerals, Metals & Materials Society, 1991. ISBN 9780873393522.

[54] E. Guo, F. Xu, and E.A. Loria. Comparison of γ/γ" precipitates and mechanical properties in modified 718 alloys. In *Superalloys 718, 625 and Various Derivatives*, pages 397–408. The Minerals, Metals & Materials Society, 1991. ISBN 9780873393522.

[55] S. Mannan, E. Hibner, and B. Puckett. Physical metallurgy of alloys 718, 725, 725hs, 925 for service in aggressive corrosive environments. Technical report, Special Metals, 2003.

[56] F. Rizzo and J.D. Buzzanell. Effect of chemistry variations on the structural stability of alloy 718. *Superalloys 1968*, pages 501–543, 1968.

[57] J. Radavich and D.J. Meyers. Thermomechanical Processing of P/M Alloy 718. *Superalloys 1984*, pages 347–356, 1984.

[58] X. Xie, X. Liu, Y. Hu, B. Tang, Z. Xu, J. Dong, K. Ni, Y. Zhu, S. Tien, L. Zhang, and W. Xie. The role of phosphorus and sulfur in inconel 718. In *Superalloys 1996*, pages 599–606. The Minerals, Metals & Materials Society, 1996. ISBN 9780873393522.

[59] S.A. Loewenkamp and J.F. Radavich. Microstructure and properties of Ni-Fe base Ta-718. *Superalloys 1988*, pages 53–61, 1988.

[60] P.N. Quested, M. Mclean, and M.R. Winstone. Evaluation of electron-beam, cold hearth refining (EBHCR) of virgin and revert IN738LC. *Superalloys 1988*, pages 387–396, 1988.

[61] D.C. Seib. Stress rupture behavior of waspaloy an in-738lc at 600c (1112f) in low oxygen gaseous environments containing sulfur. In *Superalloys 2000*, pages 535–544. The Minerals, Metals & Materials Society, 2000. ISBN 9780873394772.

[62] S.W.K. Shaw. Response of in-939 to process variations. In *Superalloys 1980*, pages 275–284. The Minerals, Metals & Materials Society, 1980. ISBN 9780871701022.

[63] G. Sjoeberg, D. Imamovic, J. Gabel, O. Caballero, J.W. Brooks, J.P. Ferte, and A. Lugan. Evaluation of the in 939 alloy for large aircraft engine structures. In *Superalloys 2004*, pages 441–450. The Minerals, Metals & Materials Society, 2004. ISBN 9780873395762.

[64] M. Nganbe and M. Heilmaier. High temperature strength and failure of the Ni-base superalloy PM3030. *International Journal of Plasticity*, 25: 822–837, 2009.

[65] M. Kaufman. Properties of cast mar-m-247 for turbine blisk applications. *Superalloys 1984*, pages 43–52, 1984.

[66] R.D. Eng and D.J. Evans. High strength hip consolidated merl 76 disks. In *Superalloys 1980*, pages 491–500. The Minerals, Metals & Materials Society, 1980. ISBN 9780871701022.

[67] J. Brinegar, L.F. Norris, and L. Rozenberg. Microcast-x fine grain casting - a progress report. *Superalloys 1984*, pages 23–32, 1984.

[68] Special Metals. Nimonic alloy 263,. Technical report, Special Metals, 1971. URL `www.specialmetals.com`.

[69] D. Locq, M. Marty, and P. Caron. Optimisation of the mechanical properties of a new pm superalloy for disk applications. In *Superalloys 2000*, pages 395–403. The Minerals, Metals & Materials Society, 2000. ISBN 9780873394772.

[70] J.F. Barker and E.H. VanDerMolen. Effect of processing variables on powder metallurgy Rene '95. *Superalloys 1972*, pages 1–23, 1972.

[71] D.W. Hunt. *The stability & mechanical properties of a nickel-base turbine disc alloy*. PhD thesis, Emmanuel College, University of Cambridge, 2001.

[72] E. Wanner and D. DeAntonio. Development of a new improved controlled thermal expansion superalloy with improved oxidation resistance. In *Superalloys 1992*, pages 237–246. The Minerals, Metals & Materials Society, 1992. ISBN 9780873391894.

[73] J.K. Tien, J. Collier, P. Bretz, and B.C. Hendrix. *High Temperature Materials for Power Engineering*, chapter Raising the high temperature limit of IN718-designing Ticolloy, pages 1341–1348. Kluwer Academic Publishers, 1990. ISBN 0-7923-0925-1.

[74] Y.F. Gu, C. Cui, H. Harada, T. Fukuda, D. Ping, A. Mitsuhashi, K. Kato, T. Kobayashi, and J. Fujioka. Development of ni-co base alloys for high-temperature disk applications. In *Superalloys 2008*, pages 53–61. The Minerals, Metals & Materials Society, 2008. ISBN 9780873397285.

[75] R. Couturier, H. Burlet, S. Terzi, S. Dubiez, L. Guetaz, and Raisson G. Process development and mechanical properties of alloy u720li for high temperature turbine disks. In *Superalloys 2004*, pages 351–359. The Minerals, Metals & Materials Society, 2004. ISBN 9780873395762.

[76] F.E. Sczerzenie and G.E. Maurer. Development of Udimet 720 for high strength disk applications. *Superalloys 1984*, pages 573–580, 1984.

[77] S.K. Jain, B. Ewing, and C.A. Yin. The development of improved performance p/m udimet 720 turbine disks. In *Superalloys 2000*, pages 785–794. The Minerals, Metals & Materials Society, 2000. ISBN 9780873394772.

[78] K.A. Green. Development of isothermally forged p/m 720 for turbine disk applications. In *Superalloys 1996*, pages 697–703. The Minerals, Metals & Materials Society, 1996. ISBN 9780873393522.

[79] D. Furrer and H.J. Fecht. Microstructure and mechanical property development in superalloy 720li. In *Superalloys 2000*, pages 415–424. The Minerals, Metals & Materials Society, 2000. ISBN 9780873394772.

[80] A. Ferrari. Effect of microstructure on the early stages of creep deformation of an experimental nickel base alloy. *Superalloys 1976*, pages 201–213, 1976.

[81] G. Raisson and Y. Honnorat. P.M. superalloy for high temperature components. *Superalloys 1976*, pages 473–482, 1976.

[82] E.G. Richards and R.M. Cook. Factors influencing the stability of nickel-base high-temperature alloys. *Superalloys 1968*, pages 1–24, 1968.

[83] G. Maurer, L. Jackman, and J. Domingue. Role of cobalt in waspaloy. In *Superalloys 1980*, pages 43–52. The Minerals, Metals & Materials Society, 1980. ISBN 9780871701022.

[84] A. Sato, C. Yu-Lung, and R.C. Reed. Oxidation of nickel-based single crystal superalloys for industrial gas turbine applications. *Acta Materialia*, 59:225–240, 2010.

[85] A. Encinas-Oropesa, G.L. Drew, M.C. Hardy, A.J. Leggett, J.R. Nicholls, and N.J. Simms. Effects of oxidation and hot corrosion in a nickel disc alloy. In *Superalloys 2008*, pages 609–618. The Minerals, Metals & Materials Society, 2008. ISBN 9780873397285.

[86] J. Gayda, P. Kantzos, and J. Miller. Quench crack behavior of nickel-base disk superalloys. *NASA/TM*, 2002.

[87] B.D. Conduit, G.J. Conduit, H.J. Stone, and M.C. Hardy. Development of a new nickel based superalloy for a combustor liner and other high temperature applications. Patent GB1408536, 2014.

[88] B.D. Conduit, G.J. Conduit, H.J. Stone, and M.C. Hardy. Molybdenum-hafnium alloys for high temperature applications. Patent EP14161255, US 2014/223465, 2014.

[89] B.D. Conduit, G.J. Conduit, H.J. Stone, and M.C. Hardy. Molybdenum-niobium alloys for high temperature applications. Patent EP14161529, US 2014/224885, 2014.

[90] American Elements. Element catalogue, 2013. URL `https://www.americanelements.com`.